Complete Excitation of Discrete Quantum Systems by Single Free Electrons

F. Javier García de Abajo,[1,2,*] Eduardo J. C. Dias,[1] and Valerio Di Giulio[1]
[1]ICFO-Institut de Ciencies Fotoniques, The Barcelona Institute of Science and Technology, 08860 Castelldefels (Barcelona), Spain
[2]ICREA-Institució Catalana de Recerca i Estudis Avançats, Passeig Lluís Companys 23, 08010 Barcelona, Spain

(Received 20 February 2022; accepted 26 July 2022; published 26 August 2022)

We reveal a wealth of nonlinear and recoil effects in the interaction between individual low-energy electrons ($\lesssim$100 eV) and samples comprising a discrete number of states. Adopting a quantum theoretical description of combined free-electron and two-level systems, we find a maximum achievable excitation probability of 100%, which requires specific conditions relating to the coupling strength and the transition symmetry, as we illustrate through calculations for dipolar and quadrupolar modes. Strong recoil effects are observed when the kinetic energy of the probe lies close to the transition threshold, although the associated probability remains independent of the electron wave function even when fully accounting for nonlinear interactions with arbitrarily complex multilevel samples. Our work reveals the potential of free electrons to control localized excitations and delineates the boundaries of such control.

DOI: 10.1103/PhysRevLett.129.093401

Free-electron beams (e-beams) allow us to image material nanostructures and their excitations with an unsurpassed combination of space-energy resolution in the subangstrom-meV domain thanks to a sustained series of advances in electron microscope instrumentation over the past decades [1–9]. In particular, electron energy-loss spectroscopy (EELS) is widely used to identify localized excitations and map their spatial distributions with atomic precision [3,6,9–16], as exemplified by recent studies of photon confinement in optical cavities [17–19], atomic vibrations in thin layers [6,9,15] and molecules [7,20,21], and collective excitations such as phonon polaritons [3,4,22,23] and plasmons [8,24–27].

At e-beam energies > 30 keV, typically employed in transmission electron microscopes to perform EELS analyses, the per-electron excitation probability of each individual mode in the specimen lies several orders of magnitude below unity. While such weak interaction is beneficial to grant us clean access into the nanoscale optical response over a wide spectral range (10^{-3}–10^{3} eV), a low excitation probability also implies that we operate in the linear regime (i.e., the e-beam does not drive nonlinear dynamics, such as the creation of multiple excitations by a single electron). This situation changes when resorting to less energetic probes like those available in low-energy electron microscopes [28,29], as well as for ions and positrons used in the past to study elastic and inelastic scattering in atomic gases [30–39]. Indeed, individual $\lesssim$100 eV electrons are predicted to generate multiple excitations of a single optical mode by appropriately adjusting the beam energy [40], while the onset of anharmonic response in this regime is expected to produce mode saturation and spectral shifts [41]. In a different approach, femtosecond resolution is currently achieved in ultrafast electron microscopy by synchronizing laser and electron pulses in their arrival at the sampled structure [17,18,42–46], a method that potentially enables the determination of nonlinear response functions with nanoscale resolution [47].

Many of the aforementioned studies focus on bosonic excitations (e.g., phonons [3,4,22,23] and plasmons [8,24–27]), which exhibit the characteristic linear response of harmonic oscillators, unless strong external fields are introduced to drive them beyond the parabolic potential region. In the opposite extreme, two- and few-level (fermionic) systems display a paradigmatic nonlinear behavior, whereby a given excitation can block subsequent ones. As an example, the discreteness of energy levels in nanographenes permeates their optical response and enables nonlinear interactions at the single-free-electron level [41]. Nevertheless, fermionic excitations in systems such as atoms, molecules, and defect states in solids possess a weak transition strength that is essentially limited by the f-sum rule [48,49] and, therefore, demands the use of low-energy electrons to yield measurable inelastic scattering signals.

Nonlinear effects open fundamental questions, such as whether an individual electron can produce a given excitation with 100% probability, as well as the role of the electron wave function in determining that probability. In addition, we expect different behavior between excitations of bosonic and fermionic character in the high-coupling regime. Because the probe energies required to reach a sizable interaction strength are likely comparable to the transition energies, recoil effects (i.e., corrections to the energy transfer beyond a linear dependence in the momentum transfer) are also anticipated to play an important role. These are relevant problems of the yet poorly explored terrain of nonlinear and recoil phenomena taking place during the interaction of free electrons with localized excitations.

In this Letter, we show that a free electron can excite a two-level system with 100% probability, provided the transition symmetry and interaction strength meet specific conditions. Based on a quantum description of free electrons and localized excitations that rigorously incorporates nonlinear and recoil effects, we show that the excitation probability is independent of the electron wave function profile. Our calculations for bosonic and fermionic systems also demonstrate that recoil effects are irrelevant unless the electron energy is only a few times larger than the transition energy. Besides their fundamental interest, our results suggest a way to control localized excitations by means of free electrons, while establishing universal rules for the maximum achievable probability depending on the symmetry of the excitation and the electron-sample coupling strength, which could be beneficial for several applications such as quantum tomography [51].

Nonperturbative excitation probability including recoil.— We consider a collimated e-beam focused down to a small lateral size (e.g., ∼1 nm for 100 eV electrons and a numerical aperture ∼0.1 in the electron optics) at the region of interaction with the sampled structure, such that we can ignore its dynamics in a plane perpendicular to the beam direction z. We further assume a nonlossy specimen [i.e., characterized by excitations of large lifetime compared with the interaction time (< 2 fs for 100 eV electrons and a 10 nm sample)] comprising a discrete set of states $|j\rangle$ of energies $\hbar\omega_j$ and initially prepared in the ground state $|0\rangle$. The Hamiltonian of the combined electron-sample system can be written as

$$\hat{\mathcal{H}} = \hbar\int dq\varepsilon_q|q\rangle\langle q| + \hbar\sum_j \omega_j|j\rangle\langle j| + \hbar\int dq\int dq'\sum_{jj'} G_{qj,q'j'}|qj\rangle\langle q'j'|,$$

where the electron is represented by orthonormal momentum states $|q\rangle$ of energies $\hbar\varepsilon_q$, whereas $G_{qj,q'j'}$ are electron-sample coupling coefficients. We note that the electron momentum component $\hbar q$ parallel to the e-beam can take both positive and negative values corresponding to forward and backward motion, respectively. Expanding the wave function of the combined system as

$$|\Psi(t)\rangle = \int dq\sum_j e^{-i(\varepsilon_q+\omega_j)t}\alpha_{qj}(t)|qj\rangle,$$

inserting it into the Schrödinder equation $\hat{\mathcal{H}}|\Psi(t)\rangle = i\hbar|\dot{\Psi}(t)\rangle$, and adopting the initial conditions $\alpha_{qj}(-\infty) = \alpha_q^0\delta_{j0}$ [i.e., with the specimen in the ground state $j=0$ and an incident electron wave function $\psi^0(z,t) \propto \int dq\alpha_q^0 e^{i(qz-\varepsilon_q t)}$], we find the postinteraction solution [see Supplemental Material (SM) [52]],

$$\alpha_{qj}(\infty) = \alpha_q^0\delta_{j0} - 2\pi i\frac{M_{q\tilde{q}_j,j}}{v_{\tilde{q}_j}}\alpha^0_{\tilde{q}_j}, \tag{1}$$

where the coefficients $M_{qq',j}$ are independent of the incident electron state and satisfy the self-consistent relation

$$M_{qq',j} = G_{qj,q'0} - \int dq''\sum_{j'}\frac{G_{qj,q''j'}M_{q''q',j'}}{\varepsilon_{q''q'}+\omega_{j'0}-i0^+} \tag{2}$$

(having the form of the Lippmann-Schwinger equation [53]) with $\varepsilon_{qq'} = \varepsilon_q - \varepsilon_{q'}$, $\omega_{jj'} = \omega_j - \omega_{j'}$, and 0^+ representing a positive infinitesimal. Here, $v_q = d\varepsilon_q/dq$ is the group velocity of the q electron component, while $\tilde{q}_j$ represents the incident electron wave vector transitioning to q after the sample is excited from 0 to j. More precisely, $\tilde{q}_j$ is implicitly defined by $\varepsilon_{\tilde{q}_j} = \varepsilon_q + \omega_{j0}$ with $\tilde{q}_j > 0$ (i.e., $\alpha^0_{\tilde{q}_j}$ only contains forward propagating components).

We are interested in the probability P_j for a sampled system initially prepared in its ground state $|0\rangle$ to be left in state $|j\rangle$ after the interaction has taken place. We thus write $P_j = \int dq|\alpha_{qj}(\infty)|^2$, which upon insertion of Eq. (1) leads to a decomposition of the probability in incident-momentum components according to (see SM [52])

$$P_j = \int_{q^j_{\min}}^{\infty} dq|\alpha_q^0|^2 P_{q,j}, \tag{3}$$

where

$$P_{q,j} = \frac{4\pi^2}{v_{q_j}v_q}(|M_{q_j\,q,j}|^2 + |M_{-q_j\,q,j}|^2) \tag{4}$$

for excited states $j \neq 0$. Here, the final electron wave vector $q_j > 0$ is defined through $\varepsilon_{q_j} = \varepsilon_q - \omega_{j0}$, and a minimum incident wave vector $q^j_{\min}$ is imposed by the threshold excitation condition $\varepsilon_{q^j_{\min}} = \omega_{j0}$. The first and second terms in Eq. (4) correspond to the contributions of forward and backward electron scattering (i.e., final wave vectors q_j and $-q_j$, respectively).

The result in Eq. (3) reveals a trivial role of the incident electron wave function (i.e., not on the wave shape, but only on the incident electron spectrum): each initial wave vector component contributes to the excitation probability in proportion to $|\alpha_q^0|^2$ [see Eq. (3)], with no dependence on the phase of α_q^0 [i.e., on the profile of the incident wave function $\psi^0(z,t)$]. We remark that this conclusion is derived from a nonperturbative formalism that rigorously accounts for nonlinear and recoil effects.

Because the energy spread of the incident beam plays a trivial role, we limit our discussion to monochromatic electrons of energy $\hbar\varepsilon_{q_0}$ with $|\alpha_q^0|^2 = \delta(q-q_0)$, so that the excitation probability reduces to $P_j = P_{q_0,j}$, subject to the condition $q_0 > q^j_{\min}$. In addition, we focus on two-level

systems, although the present formalism can be readily applied to multilevel configurations. We thus concentrate on the excitation probability P_1 and also consider the linear probability P_1^{lin} for reference, obtained from Eqs. (2) and (4) by neglecting the integral term in the former (see SM [52]).

Pointlike interaction limit.—As a first tutorial step, we obtain a closed-form solution when the interaction is localized to just one point, so that the coupling coefficients $G_{qj,q'j'}$ are independent of q and q'. Then, the excitation probability reduces to (see SM [52])

$$P_1 = \frac{P_1^{\mathrm{lin}}}{(1 + P_1^{\mathrm{lin}}/2)^2},$$

which presents a single maximum $P_1 = 1/2$ as a function of the linear probability at $P_1^{\mathrm{lin}} = 2$, as shown in Fig. 1. We include backscattering in the linear probability only for this case. This result already reveals that maximum excitation is only achieved for a very specific value of the coupling coefficient or, alternatively, a concrete value of P_1^{lin}. Interestingly, the presence of two inelastic channels (forward and backward scattering) limits the maximum probability to 50%. Indeed, if we disregard backscattering, which should be reasonable for energetic electrons, a similar analysis leads to (see SM [52])

$$P_1 = \frac{P_1^{\mathrm{lin}}}{(1 + P_1^{\mathrm{lin}}/4)^2},$$

whose maximum value is now $P_1 = 1$, obtained at $P_1^{\mathrm{lin}} = 4$. For comparison, we show the $P_1 = P_1^{\mathrm{lin}}$ line corresponding to a bosonic mode, and obviously, all of these results are in mutual agreement in the $P_1^{\mathrm{lin}} \ll 1$ limit. Incidentally, the average population of the excited state in a two-level system interacting with many multiple uncorrelated electrons is $1/2$ [16].

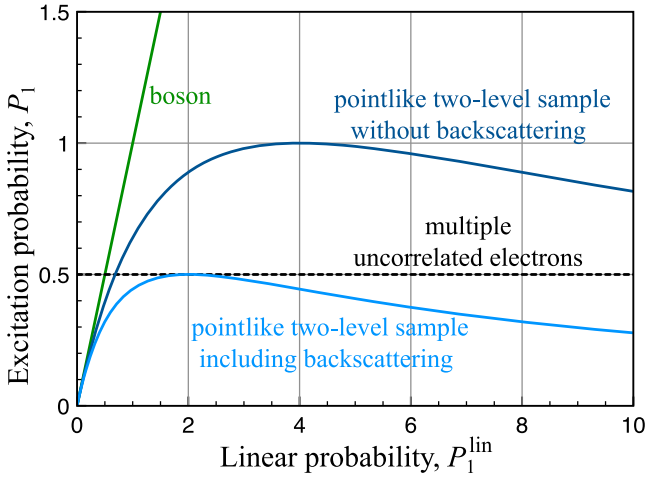

FIG. 1. Nonlinear effects in the excitation of two-level systems by a single free electron. We represent the probability P_1 as a function of the first-order (linear) probability P_1^{lin} for a lossless pointlike two-level system with and without inclusion of backscattering. The $P_1 = P_1^{\mathrm{lin}}$ probability for a bosonic excitation is also shown for comparison. Many multiple uncorrelated electrons produce a probability of $1/2$.

Nonlinear e-beam excitation without recoil.—As we show below, recoil effects can be neglected if the electron energy exceeds several times the transition energy. We can then linearize the electron energy difference as $\varepsilon_{qq'} \approx (q - q')v$, where v is the electron velocity. Considering a small sampled system, whose interaction with low-energy electrons can be described through the Coulomb potential, we find the associated coupling coefficients to only depend on the wave vector difference $q - q'$ and take the form $G_{qj,0j'} \propto (\mathrm{sgn}\{q\})^{\sigma}|q|^{l}K_m(|q|R_e)$, where R_e is the beam-sample distance, (l, m) are the angular momentum numbers associated with the excitation symmetry, σ takes values of 0 or 1, and a constant of proportionality depending on the details of the system is taken to be absorbed in P_1^{lin}. In particular, we consider excitations of dipolar [p_x and p_z, corresponding to $(l, m, \sigma) = (1, 1, 0)$ and (1,0,1), respectively] and quadrupolar [d_{z_2}, d_{xz}, and $d_{x^2-y^2}$, corresponding to (2,0,0), (2,1,1), and (2,2,0)] character, with a geometrical configuration as shown in the inset of Fig. 2(a) [see SM [52] for details and Fig. 2(b) for the associated momentum-space coupling coefficients]. We remark that, although we use an orbital notation for the excitation symmetry, this description is not restricted to atomic transitions and can be applied to plasmons and other types of localized polaritons having those symmetries, as well as to optically bright excitons and defect states (e.g., in 2D materials [58]).

Under these conditions, the wave function of the system admits the form (see SM [52])

$$\langle z|\Psi(t)\rangle = \psi^0(z,t)\sum_j f_j(z)e^{-i\omega_{j0}(z/v-t)}e^{-i\omega_j t}|j\rangle,$$

where the space-dependent functions $f_j(z)$ evolve as

$$\frac{df_j(z)}{dz} = -\frac{i}{v}\sum_{j'} G_{jj'}(z)e^{i\omega_{jj'}z/v}f_{j'}(z), \tag{5}$$

and we introduce real-space coupling coefficients $G_{jj'}(z) = \int dq G_{qj,0j'}e^{iqz}$ [see Fig. 2(a)]. Finally, the excitation probability is simply given by $P_j = |f_j(\infty)|^2$, while the linear limit reduces to $P_j^{\mathrm{lin}} = (4\pi^2/v^2)|G_{0j,\omega_{j0}/v,0}|^2$ for $j \neq 0$ (see SM [52]).

We numerically integrate Eq. (5) for two-level systems with the excitation symmetries noted above to obtain the universal plots of P_1 presented in Figs. 2(e)–2(i) as a function of the dimensionless parameters $\omega_{10}R_e/v$ and P_1^{lin}. Remarkably, we find that P_1 reaches a single maximum of 100% at a specific $(\omega_{10}R_e/v, P_1^{\mathrm{lin}})$ point [white dots in Figs. 2(e)–2(i)], thus providing a positive answer to the

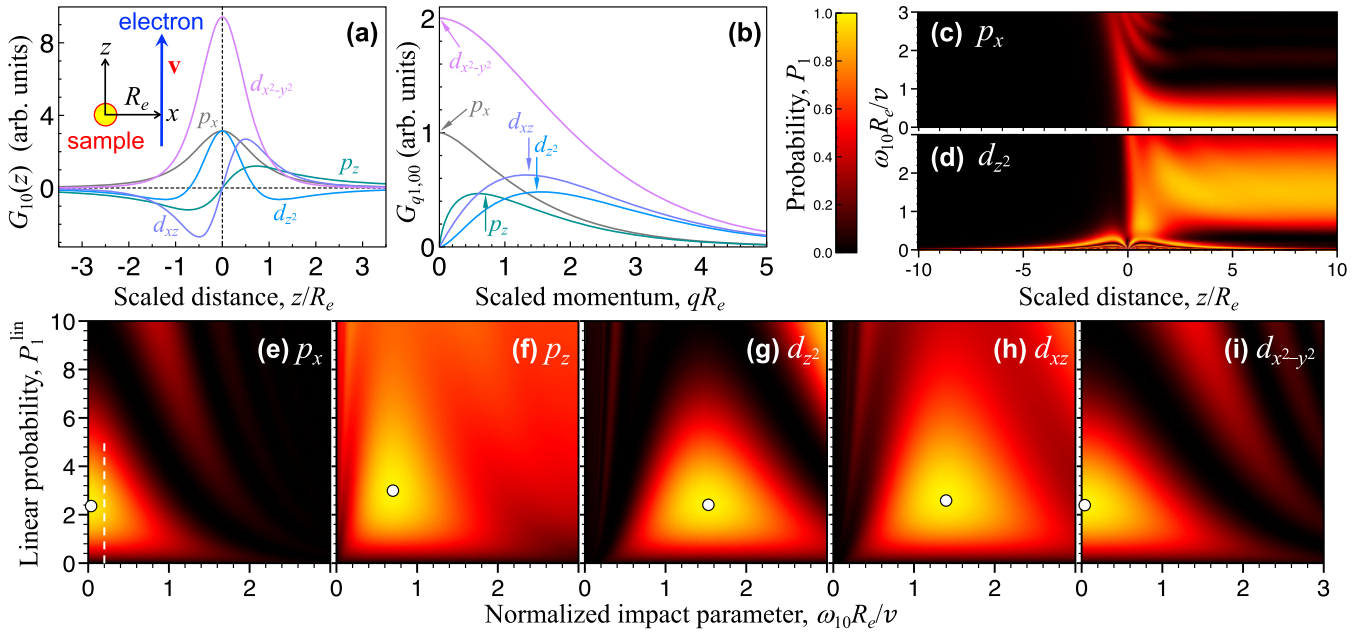

FIG. 2. Excitation of two-level systems by a single free electron. We consider the configuration illustrated in the inset of (a) and study the excitation probability for different transition symmetries. (a),(b) Electron-sample interaction coefficients $G_{10}(z)$ and $G_{q1,00}$ in the real-space (a) and momentum-space (b) representations, respectively, for dipolar (p_x and p_z) and quadrupolar (d_{z^2}, d_{xz}, and $d_{x^2-y^2}$) excitations with different angular symmetries. (c),(d) Evolution of the excited state occupation as a function of position along the electron trajectory z and impact parameter R_e for two selected dipolar and quadrupolar excitation symmetries (see labels). (e)-(i) Dependence of the postinteraction excitation probability (at $z \to \infty$) as a function of the normalized impact parameter $\omega_{10}R_e/v$ and linear probability $P_1^{\rm lin}$ for all nonvanishing dipolar and quadrupolar excitation symmetries under the investigated beam-sample configuration. The probability reaches 100% at the positions indicated by the white dots in (e)–(i). We take fixed values of $P_1^{\rm lin} = 2.5$ and 1.5 in (c) and (d), respectively. The vertical dashed line in (e) corresponds to the value $\omega_{10}R_e/v = 0.2$ used in Fig. 3(a).

question posed in the introduction, although complete excitation requires very specific conditions to take place. The position of this maximum occurs at values of $P_1^{\rm lin}$ that are in the range of those obtained in the point-interaction limit (Fig. 1), while the impact parameter R_e lies close to the stationary points of $G_{q1,00}$ as a function of qR_e for a wave vector transfer $q = \omega_{10}/v$ determined by the nonrecoil approximation [cf. the maxima of the curves in Fig. 2(b) and the abscissas of the white dots in Figs. 2(e)–2(i)]. Nevertheless, we observe broad peak distributions in spatial impact parameter, thus relaxing the condition for a tightly focused e-beam. Two of the studied symmetries have this maximum at $R_e = 0$, accompanied by a lack of any zeros in the real-space profile of the corresponding coupling coefficients [Fig. 2(a)], in contrast to the other excitations under consideration. Incidentally, P_1 presents multiple maxima as we move along R_e for fixed $P_1^{\rm lin}$, the magnitudes of which decrease with increasing impact parameter. This is the result of a complex evolution of the position-dependent probability $|f_1(z)|^2$ along the electron path, which exhibits oscillations before reaching an asymptotic value of P_1 at large z [see examples of this dynamics in Figs. 2(c) and 2(d)].

Interestingly, in the nonrecoil approximation, the deexcitation probability of a two-level system initially prepared

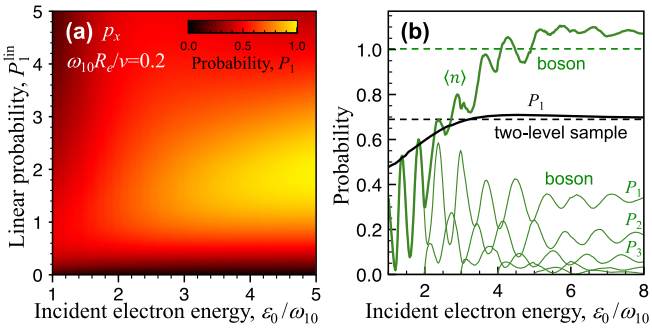

FIG. 3. Recoil effects in near-edge excitation. (a) Excitation probability P_1 for a two-level sample as a function of incident electron energy (horizontal axis, normalized to the excitation energy $\hbar\omega_{10}$) and linear excitation probability $P_1^{\rm lin}$. We consider dipolar excitations of p_x symmetry and a normalized impact parameter $\omega_{10}R_e/v = 0.2$ [i.e., corresponding to conditions along the vertical white dashed line in Fig. 2(e) in the nonrecoil limit]. (b) Probability extracted from (a) for fixed $P_1^{\rm lin} = 1$ (black curve) compared with the excitation probability for a bosonic mode with the same $0 \to 1$ matrix element (green curves, comprising a decomposition in the contributions P_n of different Fock states $|n\rangle$, as well as the final average population $\langle n \rangle = \sum_{n=1}^{\infty} nP_n$). Dashed curves indicate the $\varepsilon_0 \gg \omega_{10}$ nonrecoil limit.

in the excited state (e.g., via previous exposure to a laser π pulse) is fully identical to the excitation probability starting from the ground state (see demonstration in SM [52]), and therefore, 100% deexcitation is also predicted.

Effect of electron recoil.—The solution of Eqs. (2) and (4) for a two-level system produces an excitation probability that is substantially reduced with respect to the nonrecoil limit when the incident electron energy $\hbar\varepsilon_0$ approaches the excitation threshold $\hbar\omega_{10}$. We illustrate this effect in Fig. 3(a) for $\omega_{10}R_e/v = 0.2$ and p_x transition symmetry over a wide range of coupling strengths (vertical axis), but we find that this conclusion is general upon extensive numerical inspection of different R_e values. The nonrecoil result is however recovered when ε_0 is just a few times ω_{10}. A similar effect of recoil is observed in the excitation of a bosonic mode [Fig. 3(b)], although the interplay between different Fock states $|n\rangle$ leads to a more complex evolution characterized by sharp oscillations in both the total excitation probability and the partial contribution coming from each $|n\rangle$ state. These oscillations are attenuated as ε_0 increases, leading to a Poissonian distribution [40,54] (see also SM [52]).

We also find that recoil breaks the aforementioned excitation-deexcitation symmetry in a two-level system, particularly when $\varepsilon_0/\omega_{10}$ approaches 1 (see Fig. S1 in SM [52]).

In summary, a wealth of phenomena unfolds from the interaction between free electrons and few-level systems. Remarkably, the excitation probability is independent of the shape of the electron wave function even when nonlinear and recoil effects are rigorously accounted for. In addition, complete excitation of a two-level system by an individual electron is possible, but it requires specific interaction conditions that depend on the symmetry of the excited mode. Low-energy electrons in the < 100 eV range are promising to explore these effects, as they can generate multiple excitations of a single plasmon mode in atomically thin nanostructures [40]. Excitons in two-dimensional materials [59] offer a potentially practical candidate to study the interaction of free electrons with few-level systems, while defect states in those materials, already explored with electron tunneling microscopy [58], are robust two-level systems that could be investigated with low-energy electrons in a reflection configuration. For low-energy electrons aimed at a solid surface, reflection could be incorporated as an extension of the present analysis from plane waves to low-energy electron-diffraction-like states [60]. Free-electron interaction with diluted atomic or molecular gases could also serve as a platform to study the coupling strength, continuing previous efforts on low-energy electron, ion, and positron collisions with atomic gases [30–39]. As an exciting direction, incipient electron microscopy studies on optical atomic lattices and condensates [61] could be extended to measure inelastic scattering and explore the physics portrayed in the present work.

This work has been supported in part by the European Research Council (Advanced Grant No. 789104-eNANO), the European Commission (Horizon 2020 Grants No. 101017720 FET-Proactive EBEAM and No. 964591-SMART-electron), the Spanish MICINN (PID2020–112625 GB-I00 and Severo Ochoa CEX2019-000910-S), the Catalan CERCA Program, and Fundaciós Cellex and Mir-Puig.

*javier.garciadeabajo@nanophotonics.es

[1] P. D. Nellist and S. J. Pennycook, Subangstrom Resolution by Underfocused Incoherent Transmission Electron Microscopy, Phys. Rev. Lett. **81**, 4156 (1998).
[2] P. E. Batson, N. Dellby, and O. L. Krivanek, Sub-ångstrom resolution using aberration corrected electron optics, Nature (London) **418**, 617 (2002).
[3] O. L. Krivanek, T. C. Lovejoy, N. Dellby, T. Aoki, R. W. Carpenter, P. Rez, E. Soignard, J. Zhu, P. E. Batson, M. J. Lagos, R. F. Egerton, and P. A. Crozier, Vibrational spectroscopy in the electron microscope, Nature (London) **514**, 209 (2014).
[4] M. J. Lagos, A. Trügler, U. Hohenester, and P. E. Batson, Mapping vibrational surface and bulk modes in a single nanocube, Nature (London) **543**, 529 (2017).
[5] O. L. Krivanek, N. Dellby, J. A. Hachtel, J.-C. Idrobo, M. T. Hotz, B. Plotkin-Swing, N. J. Bacon, A. L. Bleloch, G. J. Corbin, M. V. Hoffman, C. E. Meyer, and T. C. Lovejoy, Progress in ultrahigh energy resolution EELS, Ultramicroscopy **203**, 60 (2019).
[6] F. S. Hage, G. Radtke, D. M. Kepaptsoglou, M. Lazzeri, and Q. M. Ramasse, Single-atom vibrational spectroscopy in the scanning transmission electron microscope, Science **367**, 1124 (2020).
[7] J. A. Hachtel, J. Huang, I. Popovs, S. Jansone-Popova, J. K. Keum, J. Jakowski, T. C. Lovejoy, N. Dellby, O. L. Krivanek, and J. C. Idrobo, Identification of site-specific isotopic labels by vibrational spectroscopy in the electron microscope, Science **363**, 525 (2019).
[8] V. Mkhitaryan, K. March, E. Tseng, X. Li, L. Scarabelli, L. M. Liz-Marzán, S.-Y. Chen, L. H. G. Tizei, O. Stéphan, J.-M. Song, M. Kociak, F. J. García de Abajo, and A. Gloter, Can copper nanostructures sustain high-quality plasmons?, Nano Lett. **21**, 2444 (2021).
[9] X. Yan, C. Liu, C. A. Gadre, L. Gu, T. A., T. C. Lovejoy, N. Dellby, O. L. Krivanek, D. G. Schlom, R. Wu, and X. Pan, Single-defect phonons imaged by electron microscopy, Nature (London) **589**, 65 (2021).
[10] R. F. Egerton, *Electron Energy-loss Spectroscopy in the Electron Microscope* (Plenum Press, New York, 1996).
[11] R. F. Egerton, New techniques in electron energy-loss spectroscopy and energy-filtered imaging, Micron **34**, 127 (2003).
[12] R. Erni and N. D. Browning, Valence electron energy-loss spectroscopy in monochromated scanning transmission electron microscopy, Ultramicroscopy **104**, 176 (2005).
[13] R. Brydson, *Electron Energy Loss Spectroscopy* (BIOS Scientific Publishers, Oxford, 2001).
[14] F. J. García de Abajo, Optical excitations in electron microscopy, Rev. Mod. Phys. **82**, 209 (2010).

[15] F. S. Hage, R. J. Nicholls, J. R. Yates, D. G. McCulloch, T. C. Lovejoy, N. Dellby, O. L. Krivanek, K. Refson, and Q. M. Ramasse, Nanoscale momentum-resolved vibrational spectroscopy, Sci. Adv. **4**, eaar7495 (2018).

[16] F. J. García de Abajo and V. Di Giulio, Optical excitations with electron beams: Challenges and opportunities, ACS Photonics **8**, 945 (2021).

[17] O. Kfir, H. Lourenço-Martins, G. Storeck, M. Sivis, T. R. Harvey, T. J. Kippenberg, A. Feist, and C. Ropers, Controlling free electrons with optical whispering-gallery modes, Nature (London) **582**, 46 (2020).

[18] K. Wang, R. Dahan, M. Shentcis, Y. Kauffmann, A. Ben Hayun, O. Reinhardt, S. Tsesses, and I. Kaminer, Coherent interaction between free electrons and a photonic cavity, Nature (London) **582**, 50 (2020).

[19] Y. Auad, C. Hamon, M. Tencé, H. Lourenço-Martins, V. Mkhitaryan, O. Stéphan, F. J. García de Abajo, L. H. G. Tizei, and M. Kociak, Unveiling the coupling of single metallic nanoparticles to whispering-gallery microcavities, Nano Lett. **22**, 319 (2022).

[20] P. Rez, T. Aoki, K. March, D. Gur, O. L. Krivanek, N. Dellby, T. C. Lovejoy, S. G. Wolf, and H. Cohen, Damage-free vibrational spectroscopy of biological materials in the electron microscope, Nat. Commun. **7**, 10945 (2016).

[21] D. M. Haiber and P. A. Crozier, Nanoscale probing of local hydrogen heterogeneity in disordered carbon nitrides with vibrational electron energy-loss spectroscopy, ACS Nano **12**, 5463 (2018).

[22] N. Li, X. Guo, X. Yang, R. Qi, T. Qiao, Y. Li, R. Shi, Y. Li, K. Liu, Z. Xu, L. Liu, F. J. García de Abajo, Q. Dai, E.-G. Wang, and P. Gao, Direct observation of highly confined phonon polaritons in suspended monolayer hexagonal boron nitride, Nat. Mater. **20**, 43 (2021).

[23] A. Konečná, J. Li, J. H. Edgar, F. J. García de Abajo, and J. A. Hachtel, Revealing nanoscale confinement effects on hyperbolic phonon polaritons with an electron beam, Small **17**, 2103404 (2021).

[24] M. Bosman, V. J. Keast, M. Watanabe, A. I. Maaroof, and M. B. Cortie, Mapping surface plasmons at the nanometre scale with an electron beam, Nanotechnology **18**, 165505 (2007).

[25] J. Nelayah, M. Kociak, O. Stéphan, F. J. García de Abajo, M. Tencé, L. Henrard, D. Taverna, I. Pastoriza-Santos, L. M. Liz-Marzán, and C. Colliex, Mapping surface plasmons on a single metallic nanoparticle, Nat. Phys. **3**, 348 (2007).

[26] David Rossouw and Gianluigi A. Botton, Plasmonic Response of Bent Silver Nanowires for Nanophotonic Subwavelength Waveguiding, Phys. Rev. Lett. **110**, 066801 (2013).

[27] S. F. Tan, L. Wu, J. K. W. Yang, P. Bai, M. Bosman, and C. A. Nijhuis, Quantum plasmon resonances controlled by molecular tunnel junctions, Science **343**, 1496 (2014).

[28] M. Rocca, Low-energy EELS investigation of surface electronic excitations on metals, Surf. Sci. Rep. **22**, 1 (1995).

[29] R. Tromp, Spectroscopy with the low energy electron microscope, in *Handbook of Microscopy*, edited by P. W. Hawkes and J. C. H. Spence (Springer, Berlin, 2019), pp. 565–604.

[30] E. E. Muschlitz Jr., T. L. Bailey, and J. H. Simons, Elastic and inelastic scattering of low-velocity H^- ions in hydrogen, J. Chem. Phys. **24**, 1202 (1956).

[31] W. H. Cramer and J. H. Simons, Elastic and inelastic scattering of low-velocity He^+ ions in helium*, J. Chem. Phys. **26**, 1272 (1957).

[32] H. H. Farrell and M. Strongin, Scattering of low-energy electrons from rare-gas crystals grown on the (100) face of Nb. II. Inelastic scattering and energy-loss spectra, Phys. Rev. B **6**, 4711 (1972).

[33] M. Barat, D. Dhuicq, R. François, and V. Sidis, Elastic and inelastic scattering of Li^+ ions by rare gases (Ne, Ar, Kr, Xe), J. Phys. B: At. Mol. Opt. Phys. **6**, 2072 (1973).

[34] S. M. Kazakov, A. I. Korotkov, and O. B. Shpenik, Resonant scattering of low-energy electrons by mercury atoms, Sov. Phys. JETP **51**, 847 (1980), http://www.jetp.ras.ru/cgi-bin/dn/e_051_05_0847.pdf.

[35] K. Tachibana, Excitation of the $1s_5$, $1s_4$, $1s_3$, and $1s_2$ levels of argon by low-energy electrons, Phys. Rev. A **34**, 1007 (1986).

[36] J. Berkowitz, Sum rules and the photoabsorption cross sections of C_{60}, J. Chem. Phys. **111**, 1446 (1999).

[37] M. Kitajima, M. Okamoto, K. Sunohara, H. Tanaka, H. Cho, S. Samukawa, S. Eden, and N. J. Mason, Low-energy electron impact elastic and inelastic scattering from CF_3I, J. Phys. B **35**, 3257 (2002).

[38] R. A. Boadle, T. J. Babij, J. R. Machacek, R. P. McEachran, J. P. Sullivan, and S. J. Buckman, Low-energy elastic and inelastic scattering of positrons from argon, Phys. Rev. A **93**, 022712 (2016).

[39] H. Tanaka, M. Hoshino, and M. J. Brunger, Elastic and inelastic scattering of low-energy electrons from gas-phase C_{60}: elastic scattering angular distributions and coexisting solid-state features revisited, Eur. Phys. J. D **75**, 293 (2021).

[40] F. J. García de Abajo, Multiple excitation of confined graphene plasmons by single free electrons, ACS Nano **7**, 11409 (2013).

[41] J. D. Cox and F. J. García de Abajo, Nonlinear interactions between free electrons and nanographenes, Nano Lett. **20**, 4792 (2020).

[42] B. Barwick, D. J. Flannigan, and A. H. Zewail, Photon-induced near-field electron microscopy, Nature (London) **462**, 902 (2009).

[43] F. J. García de Abajo, A. Asenjo-Garcia, and M. Kociak, Multiphoton absorption and emission by interaction of swift electrons with evanescent light fields, Nano Lett. **10**, 1859 (2010).

[44] A. Feist, K. E. Echternkamp, J. Schauss, S. V. Yalunin, S. Schäfer, and C. Ropers, Quantum coherent optical phase modulation in an ultrafast transmission electron microscope, Nature (London) **521**, 200 (2015).

[45] L. Piazza, T. T. A. Lummen, E. Quiñonez, Y. Murooka, B. W. Reed, B. Barwick, and F. Carbone, Simultaneous observation of the quantization and the interference pattern of a plasmonic near-field, Nat. Commun. **6**, 6407 (2015).

[46] J.-W. Henke, A. Sajid Raja, A. Feist, G. Huang, G. Arend, Y. Yang, F. J. Kappert, R. Ning Wang, M. Möller, J. Pan, J. Liu, O. Kfir, C. Ropers, and T. J. Kippenberg, Integrated photonics enables continuous-beam electron phase modulation, Nature (London) **600**, 653 (2021).

[47] A. Konečná, V. Di Giulio, V. Mkhitaryan, C. Ropers, and F. J. García de Abajo, Nanoscale nonlinear spectroscopy with electron beams, ACS Photonics **7**, 1290 (2020).

[48] P. Noziéres, *Theory of Interacting Fermi Systems* (Taylor & Francis, Boca Raton, FL, 1997).

[49] For a dipolar excitation of frequency ω_0, the f-sum rule limits the transition dipole d by $d^2 \leq (\hbar e^2/2m_e\omega_0)N_e$, where N_e is the effective number of involved electrons. We have $N_e < 1$ for atomic transitions, in contrast to plasmonic excitations in metallic nanostructures, for which N_e is of the order of the number of conduction electrons [50].

[50] Z.-J. Yang, T. J. Antosiewicz, R. Verre, F. J. García de Abajo, S. P. Apell, and M. Käll, Ultimate limit of light extinction by nanophotonic structures, Nano Lett. **15**, 7633 (2015).

[51] R. Ruimy, A. Gorlach, C. Mechel, N. Rivera, and I. Kaminer, Toward Atomic-Resolution Quantum Measurements with Coherently Shaped Free Electrons, Phys. Rev. Lett. **126**, 233403 (2021).

[52] See Supplemental Material at http://link.aps.org/supplemental/10.1103/PhysRevLett.129.093401 for further details of the present formalism, which also includes Refs. [16,41,53–57].

[53] A. Messiah, *Quantum Mechanics* (North-Holland, New York, 1966).

[54] V. Di Giulio, M. Kociak, and F. J. García de Abajo, Probing quantum optical excitations with fast electrons, Optica **6**, 1524 (2019).

[55] J. D. Jackson, *Classical Electrodynamics* (Wiley, New York, 1999).

[56] F. J. García de Abajo, Relativistic energy loss and induced photon emission in the interaction of a dielectric sphere with an external electron beam, Phys. Rev. B **59**, 3095 (1999).

[57] M. Abramowitz and I. A. Stegun, *Handbook of Mathematical Functions* (Dover, New York, 1972).

[58] B. Schuler, K. A. Cochrane, C. Kastl, E. S. Barnard, E. Wong, N. J. Borys, A. M. Schwartzberg, D. F. Ogletree, F. J. García de Abajo, and A. Weber-Bargioni, Electrically driven photon emission from individual atomic defects in monolayer WS_2, Sci. Adv. **6**, eabb5988 (2020).

[59] L. H. G. Tizei, Y.-C. Lin, M. Mukai, H. Sawada, A.-Y. Lu, L.-J. Li, K. Kimoto, and K. Suenaga, Exciton Mapping at Subwavelength Scales in Two-Dimensional Materials, Phys. Rev. Lett. **114**, 107601 (2015).

[60] J. B. Pendry, *Low Energy Electron Diffraction* (Academic Press, London, 1974).

[61] T. Gericke, P. Würtz, D. Reitz, T. Langen, and H. Ott, High-resolution scanning electron microscopy of an ultracold quantum gas, Nat. Phys. **4**, 949 (2008).